Journal of Materials Chemistry A

Proton-conducting phosphate glass and its melt exhibiting high electrical conductivity at intermediate temperatures

Journal:	*Journal of Materials Chemistry A*
Manuscript ID	TA-ART-08-2018-008162.R1
Article Type:	Paper
Date Submitted by the Author:	02-Nov-2018
Complete List of Authors:	Yamaguchi, Takuya; Tohoku University, Institute of Multidisciplinary Research for Advanced Materials Tsukuda, Satoshi; Tohoku University, Institute of Multidisciplinary Research for Advanced Materials Ishiyama, Tomohiro; National Institute of Advanced Industrial Science and Technology, Nishii, Junji; Hokkaido university, Research Institute for Electronic Science Yamashita, Toshiharu; Kawazoe Frontier Technologies Corporation Kawazoe, Hiroshi; Kawazoe Frontier Technologies Corp., Omata, Takahisa; Tohoku University, IMRAM

SCHOLARONE™
Manuscripts

Proton-conducting phosphate glass and its melt exhibiting high electrical conductivity at intermediate temperatures

Takuya Yamaguchi,[a†] Satoshi Tsukuda,[a] Tomohiro Ishiyama,[b]

Junji Nishii,[c] Toshiharu Yamashita,[d] Hiroshi Kawazoe[d] and Takahisa Omata[a*]

[a] *Institute of Multidisciplinary Research for Advanced Materials, Tohoku University, Katahira 2-1-1, Sendai 980-8577, Japan*

[b] *Fuel Cell Materials Group, Research Institute for Energy Conservation, National Institute of Advanced Industrial Science and Technology (AIST), AIST Central 5, Higashi 1-1-1, Tsukuba, Ibaraki 305-8565, Japan*

[c] *Research Institute for Electronic Science, Hokkaido University, Kita 21 Nishi 10, Kita-ku, Sapporo 001-0021, Japan*

[d] *Kawazoe Frontier Technologies Corporation, Kuden-cho 931-113, Sakae-ku, Yokohama 247-0014, Japan*

* Corresponding author. Tel.: +81-22-217-5832, fax: +81-22-217-5832
e-mail: takahisa.omata.c2@tohoku.ac.jp

† Present address: Fuel Cell Materials Group, Research Institute for Energy Conservation, National Institute of Advanced Industrial Science and Technology (AIST), AIST Central 5, Higashi 1-1-1, Tsukuba, Ibaraki 305-8565, Japan

Abstract

A working hypothesis to design proton-conducting phosphate glasses exhibiting high proton conductivity and high stability was proposed. In this hypothesis, the precursor glass before electrochemical alkali-proton substitution (APS) is required to fulfill the terms of (i) the concentration of $NaO_{1/2}$ in the precursor glass needs to be higher than 35 mol%, (ii) the O/P ratio of the glass composition cannot exceed 3.5, (iii) the glass network modifier oxides need to consist of cations with low electronegativity, (iv) the glass must contain a sufficient amount of glass network modifiers and intermediate oxides, such as alkaline-earth oxides, Al_2O_3, Y_2O_3, La_2O_3, WO_3, Nb_2O_5, and Ta_2O_5, (v) the glass needs to consist of more than four or five components, and (vi) the glass must contain a small amount of GeO_2 and/or B_2O_3. Based on the proposed working hypothesis, we obtained a $36HO_{1/2}$-$4NbO_{5/2}$-2BaO-$4LaO_{3/2}$-$4GeO_2$-$1BO_{3/2}$-$49PO_{5/2}$ glass (36H-glass) by APS. While the glass transition temperature of 36H-glass was 179 °C, the glass, accurately the super cooled liquid, was stable for a long time up to 280 °C under fuel cell operating conditions and exhibited 1×10^{-3} S cm^{-1} at 280 °C, indicating that the developed working hypothesis is useful to design new proton-conducting electrolytes that work at intermediate temperatures.

1. Introduction

Intermediate-temperature fuel cells (ITFCs) that operate at 250–500 °C are expected to be next-generation fuel cells because they possess several advantages over current solid oxide fuel cells and polymer electrolyte membrane fuel cells, which operate at high and low temperatures, respectively, such as low cost, rapid start-up, long life, and capability to use bioalcohols as fuels.[1-3] A solid electrolyte exhibiting high proton conductivity at intermediate temperatures is desired to materialize ITFCs; therefore, many groups have devoted great effort to developing proton conductors. CsH_2PO_4, Y_2O_3-doped $BaZrO_3$ (BZY), and $BaCeO_3$ (BCY) are well-known strong candidates as proton conductors; however, these materials have not been used as electrolytes for ITFCs. This is because dehydration occurs and proton carriers are lost at temperatures higher than 230 °C in dry atmosphere in the case of CsH_2PO_4,[4-6] and the considerable electron–hole conduction in an oxidizing atmosphere induces serious current leakage in the cases of BZY and BCY.[7-10] Therefore, development of new solid electrolytes that exhibit high proton conductivity at intermediate temperatures still remains a major challenge.

Oxide glasses containing a large amount of protons as hydroxyl (OH) groups are promising materials for use as solid electrolytes in ITFCs because they exhibit proton conductivity along with high chemical and electrochemical stability. Among oxide glasses, phosphate glasses are especially strong candidates as solid electrolytes because they have the potential to exhibit high proton conductivity as a result of their high proton mobility arising from the strong hydrogen bonding of OH groups. Since Namikawa et al.[11] reported the proton conductivity of phosphate glasses in 1966, many groups have attempted to develop phosphate glasses that exhibit high proton conductivity.[12-16] Because most protons (OH groups) in the glasses are lost as water vapor during the high

temperature melting at 1200–1300 °C required to obtain homogeneous glasses, most previous studies focused on increasing the concentration of proton carriers in phosphate glasses.[12-16] One possible approach to increase the concentration of proton carriers is to choose a glass compositions that can be prepared at a comparatively low melting temperature such as <800 °C.[14,16] While the concentration of proton carriers in glasses prepared via high temperature melting is lower than 5×10^{20} cm^{-3}, it reached up to 8×10^{21} cm^{-3} and proton conductivity of 1×10^{-3} S cm^{-1} was attained for glasses prepared by low temperature melting.[16] However, the glass compositions that tolerate low temperature melting are limited to a narrow range around metaphosphate composition;[12-14,16] therefore, it is difficult to explore the glass compositions that exhibit high proton mobility to further increase proton conductivity.

We have recently developed a technique to inject proton carriers into phosphate glasses.[17,18] In this technique, termed alkali-proton substitution (APS), alkali ions with a concentration of ~10^{22} cm^{-3} in precursor glasses are electrochemically substituted with protons; this enables an extraordinarily high concentration of proton carriers of ~10^{22} cm^{-3} to be injected into phosphate glasses without the limitation of a narrow glass composition range.[17-24] APS is usually conducted at ~300 °C, so protons stably exist in the glasses up to ~300 °C.[21] Therefore, APS is a suitable technique to obtain phosphate glass electrolytes that exhibit high proton conductivity, i.e., high proton mobility, at intermediate temperatures.

We have prepared several proton-conducting phosphate glasses using the APS technique, and have studied the relationships between glass composition, proton mobility, and thermal stability.[20-24] Here, based on the understanding obtained from our previous studies, we propose a working hypothesis to explore the composition of glasses that

exhibit high proton conductivity and high thermal stability at intermediate temperatures. On the basis of the working hypothesis proposed here, we design $36HO_{1/2}$-$4NbO_{5/2}$-$2BaO$-$4LaO_{3/2}$-$4GeO_2$-$1BO_{3/2}$-$49PO_{5/2}$ glass (denoted as 36H-glass) as a candidate proton-conducting glass to achieve both high conductivity and high thermal stability at intermediate temperatures. The 36H-glass is prepared from the precursor $36NaO_{1/2}$-$4NbO_{5/2}$-$2BaO$-$4LaO_{3/2}$-$4GeO_2$-$1BO_{3/2}$-$49PO_{5/2}$ glass (36Na-glass), which is synthesized by the conventional melt-quenching technique, by injecting proton carriers into the precursor glass by APS. As a result, we successfully obtain a proton-conducting phosphate glass which exhibits proton conductivity of 1×10^{-3} Scm^{-1} at 280 °C stably maintained over 500 h and under fuel cell operating conditions.

2. Working hypothesis and composition design to realize both high proton conductivity and high thermal stability at intermediate temperatures

2.1. Glass composition to realize high proton conductivity

Both the carrier concentration and carrier mobility need to be high to achieve high proton conductivity, because the conductivity is proportional to these two parameters. In proton-conducting phosphate glasses prepared by APS, the concentration of proton carriers is determined by the concentration of Na^+ in the precursor glass. Therefore, the concentration of Na^+ has to be sufficiently high to inject a high concentration of protons. The concentration of proton carriers in superprotonic conductors such as $CsHSO_4$ and CsH_2PO_4 is of the order of 10^{22} cm^{-3}. Supposing that the mobility of proton carriers in amorphous materials is lower than that in crystalline phases, the proton concentration of a glass should be at least comparable with that of superprotonic conductors. Because the molar volume of phosphate glasses is generally about 20 cm^3 mol^{-1}, when the glass

compositions are expressed using cation mol%, proton carriers with a concentration of 10^{22} cm^{-3} can be injected into the glasses by APS when the precursor glass contains Na^+ with a concentration of ≥35 mol%.

The mobility of proton carriers in a glass depends on the glass structure and kinds of component oxides; i.e., glass network modifiers and intermediate oxides.[21-24] Regarding the glass structure, we previously found that the proton mobility in phosphate glasses increased as the depolymerization of the glass framework developed. This is because the energy barrier for proton migration decreases with increasing depolymerization. However, the proton mobility starts to decrease when pyrophosphate ions ($P_2O_7^{4-}$) become a major component because of their strong proton trapping, which induces a high energy barrier for proton dissociation.[24] In simple pseudo-binary systems composed of network modifier oxides and $PO_{5/2}$, the composition of a glass containing $P_2O_7^{4-}$ as a major component corresponds to the composition at which the ratio of the number of oxygen atoms to that of phosphorus atoms (the O/P ratio) is 3.5. Therefore, the upper limit of the O/P ratio to realize high proton mobility is 3.5 considering the glass network structure.

Regarding the kind of network modifier or intermediate oxide, which is another factor affecting proton mobility, we previously studied the proton mobility of $35HO_{1/2}$-5RO-$3NbO_{5/2}$-$3LaO_{3/2}$-$2GeO_2$-$2BO_{3/2}$-$50PO_{5/2}$ (R = Mg and Ba) glasses and found that the glass containing BaO exhibited a proton mobility twice that of the glass containing MgO. The O–H and P–O bonding characterization by infrared (IR) absorption and X-ray photoelectron spectroscopies showed that the glass containing electronically positive network modifiers, i.e., network modifiers with low electronegativity, exhibited high proton mobility because of the comparatively large ionicity of O–H bonds in the glass containing BaO compared with that in the glass containing MgO.[23]

Based on this understanding, we determined that the following requirements should be satisfied for a phosphate glass to exhibit high proton conductivity.

(i) The concentration of $NaO_{1/2}$ in the precursor glass should be higher than 35 mol%.

(ii) The O/P ratio of the glass composition cannot exceed 3.5.

(iii) The glass network modifier oxides contain cations with low electronegativity.

2.2 Glass compositions to realize high thermal stability at intermediate temperatures

Alkali ions in the precursor glasses are completely substituted with protons after APS. Because the coordination number of protons is unity, when the weak hydrogen bonding is removed, protons practically do not anchor phosphate glass networks to each other in contrast to the case of alkali ions. This results in a decrease of the glass transition temperature (T_g) by 150–200 °C after APS;[20,21] the maximum T_g of a glass after APS is approximately 250 °C when the precursor glass contains over 35 mol% of Na^+.[21] This means that a glass after APS is a highly viscous supercooled liquid rather than a solid at the operating temperature of ITFCs ($T \geq 250$ °C). Phase separation and crystallization of glasses are frequently observed at temperatures higher than T_g because of the faster atomic diffusion in a liquid than that in a solid. To obtain a glass suitable for use as the electrolyte in ITFCs, we therefore have to design the glass composition so that phase separation and crystallization do not occur even at temperatures above T_g (>250 °C).

One approach to suppress phase separation and crystallization at ≥250 °C is to design the composition of the precursor glass to maximize T_g. For this purpose, the precursor glass should contain a sufficient amount of network modifier and intermediate oxides that remain in the glass after APS. Considering their solubility in phosphate glasses, alkaline-earth oxides, Al_2O_3, Y_2O_3, La_2O_3, WO_3, Nb_2O_5, and Ta_2O_5 are considered to be

appropriate components of the glass to increase T_g.

Another approach to suppress phase separation and crystallization at ≥250 °C is to increase the number of components, because the supercooled liquid is stabilized by the large entropy derived from its multiple components.[25,26] In fact, commercially available glasses generally consist of more than four or five components to suppress phase separation and crystallization during production and under the conditions in which the glasses are used. In addition, we previously found that the addition of other network formers, GeO_2 and/or B_2O_3, effectively suppressed the phase separation and crystallization of the glass after APS.[20] Therefore, the additional components are not limited to network modifiers and intermediate oxides. However, the concentration of GeO_2 and/or B_2O_3 should be at most a few mole percent to maintain strong hydrogen bonding in the phosphate glass.

To summarize the above discussion, the glass compositions exhibiting high thermal stability at ≥250 °C should satisfy the following additional requirements:

(iv) The glass needs to contain a sufficient amount of glass network modifiers and intermediate oxides, such as alkaline-earth oxides, Al_2O_3, Y_2O_3, La_2O_3, WO_3, Nb_2O_5, and Ta_2O_5.

(v) The glass should consist of more than four or five components.

(vi) The glass can contain a small amount of GeO_2 and/or B_2O_3.

2.3. Design of glass composition

To meet requirement (i), we assumed an initial glass composition of $35NaO_{1/2}$-$65PO_{5/2}$. Then, to increase the thermal stability of the glass after APS, a portion of $PO_{5/2}$ was substituted with other oxides. When the nominal composition, *x*, of the additional

components, MO_x, is assumed to be 2, approximately 15 mol% of $PO_{5/2}$ can be substituted with MO_x to meet requirement (ii); this gave a composition of $35NaO_{1/2}$-$15MO_x$-$50PO_{5/2}$, which has an O/P ratio of 3.45.

To meet requirement (v), we included three kinds of additional network modifiers and intermediate oxides in the glass. One is an oxide consisting of cations with a valence state higher than three; WO_3, $NbO_{5/2}$, and $TaO_{5/2}$ are appropriate oxides. However, W^{6+} in WO_3 is reduced and forms W^{5+} and an electron in the hydrogen atmosphere during APS, resulting in electronic conduction of the glass after APS;[17,18] therefore, WO_3 is not preferred as a component of glass electrolytes. $NbO_{5/2}$ displays similar behavior; however, electronic conduction does not occur for glasses with an $NbO_{5/2}$ concentration of up to 8 mol% according to our previous study.[19] Although the reduction of Ta^{5+} in $TaO_{5/2}$ to Ta^{4+} and the formation of conduction electrons hardly occur during APS, the solubility of $TaO_{5/2}$ in phosphate glasses is not high compared to that of $NbO_{5/2}$. Therefore, $TaO_{5/2}$ is not suitable as an additional component to increase the thermal stability of the glass after APS. Based on these considerations, we used $NbO_{5/2}$ as the additional component with high-valence cations. The maximum concentration of $NbO_{5/2}$ to avoid electronic conduction of the glass after APS was determined to be 5 mol%. To meet requirement (iii), the additional oxides consisting of divalent and trivalent cations added to the glass were BaO and $LaO_{3/2}$, respectively. We determined that the total amount of BaO and $LaO_{3/2}$ should be 6 mol% to account for the addition of GeO_2 and $BO_{3/2}$ to meet requirement (vi). We included 2 mol% of BaO and 4 mol% of $LaO_{3/2}$ in the glass because of the larger ability of $LaO_{3/2}$ to increase T_g than that of BaO.[27]

To meet requirement (vi), we mainly included GeO_2, because it has a good track record of suppressing the phase separation in proton conducting glasses fabricated by APS[20] and

has a large effect to increase T_g compared to $BO_{3/2}$ (Table S1 in ESI). In addition, $BO_{3/2}$ preferably exists in the phosphate framework as tetrahedrally coordinated BO_4[28] and it probably acts as proton trap sites, because the nominal charge of BO_4 tetrahedra containing B^{3+} is −1 and this negative charge attracts positively charged protons, similar to the case of BO_4 and AlO_4 tetrahedra in SiO_2-B_2O_3 and SiO_2-Al_2O_3 zeolites.[29-32] Therefore, we included 4 mol% of GeO_2 and 1 mol% of $BO_{3/2}$ in the glass.

Finally, the precursor glass composition used in the present study was determined to be $36NaO_{1/2}$-$4NbO_{5/2}$-2BaO-$4LaO_{3/2}$-$4GeO_2$-$1BO_{3/2}$-$49PO_{5/2}$ (denoted as 36Na-glass), which has an O/P ratio of 3.43.

3. Experimental

3.1. Preparation of the precursor glass

The precursor 36Na-glass was prepared by a standard melt-quenching technique. The 36Na-glass was prepared from reagent-grade Na_2CO_3, Nb_2O_5, $BaCO_3$, La_2O_3, and H_3PO_4 (85 wt%) purchased from Wako Pure Chemical Industries Ltd., Japan, and GeO_2 and B_2O_3 purchased from Kishida Chemical Co., Ltd., Japan. These chemicals were used as received. The chemicals were weighed and mixed in a platinum crucible and then preheated at 500 °C for 60 min to remove water and CO_2 gases from the mixture. The mixture was then melted at 1400 °C for 15 min in air. The molten material was poured into a cylindrical carbon mold with an inner diameter of 18 mm preheated at 450 °C. The obtained glass was annealed at 450 °C for 20 min, and then it was cooled slowly to room temperature at a rate of 20 °C h^{-1}.

3.2. Alkali-proton substitution (APS)

The obtained cylindrical 36Na-glass was sliced into disks with a thickness of approximately 0.8 mm and then both surfaces were polished using emery paper with a grit of #800. A Pd film with a diameter of 16 mm and thickness of 100 nm was deposited on one surface of a 36Na-glass disk by magnetron sputtering (JFC-1600, JEOL, Japan). The disk was loaded onto the specimen holder of the APS apparatus (KDK-800, Kenix Co., Japan) with the Pd-coated surface facing upwards. Full details of the configuration of this apparatus are described in our previous papers.[17,18] After the temperature of the disk was increased to 332 °C in 5% H_2/95% N_2 atmosphere, the lower surface of the disk was contacted with molten Sn. Then, a DC bias of 5–10 V was applied between the Pd film and molten Sn for 6–7 h. The Pd film acted as an anode.

3.3. Characterization

The thermal expansion of the glass was recorded using a thermomechanical analyzer (SS-6000, SII, Japan) to determine its glass transition temperature (T_g) and dilatometric softening temperature (T_d). The Na concentration of the glasses before and after APS was determined using energy-dispersive X-ray spectroscopy (EDX; JED-2300, JEOL, Japan) coupled with scanning electron microscopy (SEM; JSM-6335F, JEOL, Japan). The concentration of protons forming OH groups in the glasses before and after APS was determined based on the absorbance of the O−H stretching vibration (ν_{OH}) using Fourier-transform IR spectroscopy (FT-IR6100, JASCO, Japan) and IR microscopy (IRT-5000, JASCO, Japan). The concentration of OH groups (n_{OH}, in cm^{-3}) was determined from the maximum absorption coefficient of ν_{OH} ($\alpha(\nu_{OH})$, in cm^{-1}) using the following equation:[33]

$$n_{OH} = 1.03\times10^{19}\times\alpha(\nu_{OH}). \quad (1)$$

Raman spectra of the glass samples were recorded using a laser Raman spectrometer (NRS-3100, JASCO, Japan) at an excitation wavelength of 532 nm.

3.4. Electrical properties and fuel cell test

After polishing both surfaces of the glass disk after APS, Pd film electrodes with a thickness of 50 nm were deposited on both surfaces of the disk for the electrical conductivity, electromotive force (emf), and fuel cell measurements. For the electrical conductivity measurements under various oxygen partial pressures (p_{O2}), Pt film electrodes with a thickness of 50 nm were used.

The electrical conductivity of the glass after APS at temperatures between 150 and 400 °C was measured under dry 5% H_2/95% N_2 atmosphere by the AC impedance method with an impedance analyzer (ModuLab, Solartron Analytical, UK). Electrical conductivity was measured at 280 °C under p_{O2} of 1.0×10^{-45}, 1.0×10^{-43}, 1.0×10^{-41}, 4.5×10^{-40}, 6.3×10^{-3}, 2.1×10^{-1}, and 1 atm. Mixtures of O_2 with N_2 and H_2 with N_2 were used to control p_{O2} of $\geq6.3\times10^{-3}$ and $\leq4.5\times10^{-40}$ atm, respectively. The mixed gasses were humidified by passing through water at 8 °C and the partial pressure of water in the mixed gases was fixed at 1.06×10^{-2} atm.

The mean transport number of protons was determined by emf measurements of a hydrogen concentration cell. The structure of the cell used for emf measurements was Gas (I), Pd | glass electrolyte | Pd, Gas (II). Gas (I) was fixed as pure H_2, and Gas (II) contained a mixture of H_2 and N_2 with an H_2 content of 5% to 100%. Neither Gas (I) nor Gas (II) was intentionally humidified. The fuel cell test was performed at 280 °C using the glass after APS with a thickness of 0.36 mm as an electrolyte. Dry pure H_2 gas and dry air (21% O_2/79% N_2) were supplied to the anode and cathode, respectively, at a flow

rate of 100 mL min^{-1}.

4. Results and discussion

4.1 Injection of proton carriers by APS

Fig. 1 shows the depth profiles of Na and OH concentrations in the 36Na-glass after APS. The Na and OH concentrations before APS were 1.0×10^{22} and 7.7×10^{19} cm^{-3}, respectively. In the region with a depth of 0.0–0.3 mm from the anode, almost all Na in the glass was discharged by APS. In the region with a depth of >0.3 mm from the anode, some of the Na remained after APS, and the Na concentration increased approaching the cathode. Around the cathode, approximately 20% of the Na initially contained in the glass, corresponding to 2.3×10^{21} cm^{-3}, remained. In contrast, the OH concentration in the glass after APS was 9.0×10^{21} cm^{-3} in the region with a depth of <0.3 mm from the anode. The OH concentration decreased approaching the cathode and was 7.5×10^{21} cm^{-3} around the cathode. The depth profiles of Na and OH concentrations were almost mirror images of each other; i.e., the OH concentration was low in the region where the Na concentration was high and vice versa. Quantitatively, the decrease in Na concentration ($10.0–7.7\times10^{21}$ cm^{-3}) and increase in OH concentration ($9.0–7.5\times10^{21}$ cm^{-3}) were approximately the same, indicating that protons were injected into the glass by substitution of Na^+, as was observed in previous reports.[17-24] After the part of the glass with a high remaining Na concentration was removed, the glass after APS containing the region at a depth of <0.3–0.4 mm from the anode, where Na^+ in the glass was almost completely substituted with protons, was subjected to electrical and spectroscopic measurements. Hereafter, this glass sample is termed 36H-glass.

From the thermal expansion curve of 36H-glass shown in Fig. 2, T_g and T_d of 36H-

glass were determined to be 179 °C and 230 °C, respectively. When 36H-glass is phase-separated, we observe more than one glass transition corresponding to each phase.[34,35] In Fig. 2, only one glass transition was observed; therefore, we conclude that 36H-glass is not phase-separated and consists of homogeneous single glass phase.

4.2 Proton conductivity and its time evolution

The emf of the hydrogen concentration cell at 320 °C using 36H-glass as the electrolyte, which had a structure of H_2(I), Pd | 36H-Glass | Pd, H_2(II), almost agreed with the theoretical value determined from the Nernst equation (Fig. S1 in ESI). This indicates that the mean transport number of protons in 36H-glass is unity. Fig. 3 shows an Arrhenius plot of the electrical conductivity of 36H-glass obtained in dry 5% H_2/95% N_2 atmosphere at temperatures between 150 °C and 400 °C. Because T_g of 36H-glass is 179 °C, the specimen at temperatures higher than 179 °C is not a glass but a supercooled liquid or glass melt accurately; but in the present paper, we refer to this as 36H-glass regardless of its state of matter for simplicity. The plot was linear in the temperature range from 150 °C to around 300 °C, indicating that the activation energy in this temperature range is 0.74 eV. The activation energy of proton conduction depends on the concentration of proton carriers in a glass, and the reported values for glasses with proton concentrations of $0.5–1\times10^{22}$ cm^{-3} range between 0.7 and 1.1 eV.[16,19-24] The activation energy of 36H-glass is almost the same as that of the previously reported glasses, which indicates that the proton conduction in 36H-glass originated from the hopping mechanism, similar to that of the previously reported glasses. At temperatures higher than 300 °C, the proton conductivity deviated downward from the line extrapolated from the data obtained at low temperature region. Such a downward deviation at temperatures above T_g is generally observed in alkali-ion

and Ag^+ conducting glasses, and it is explained by the temperature dependence of the viscosity of supercooled liquids.[36,37] The proton conductivity was 2×10^{-3} S cm^{-1} at 300 °C, which was the higher end of the region with a linear relationship, and 8×10^{-3} S cm^{-1} at 400 °C, which was the maximum temperature in the present measurements. These proton conductivities are the highest among reported proton-conducting phosphate glasses.[11-24] This leads to the expectation that 36H-glass will be suitable as an electrolyte in ITFCs if its proton conductivity remains stable for a long time.

Fig. 4 shows the time evolution of the proton conductivity of 36H-glass at 280, 320, 360, and 400 °C. At 400 °C, the conductivity steeply decreased during the initial 30 h; it then increased gradually over time until 110 h, and then it decreased again. At 360 °C, the conductivity of 36H-glass decreased during the initial 300 h, and then it was constant at 1×10^{-3} S cm^{-1}. At 320 °C, the conductivity decreased gradually over time. In contrast to the cases at ≥320 °C, while a slight conductivity decrease was observed in the initial 200 h, the proton conductivity was almost constant at 1×10^{-3} S cm^{-1} at 280 °C, indicating that the proton conductivity of 36H-glass is stable for a long period at 280 °C. Because the shape of the specimen did not change during the conductivity measurement at 280 °C for 555 h (Figs. S2 (a) and (b) in ESI), the glass at 280 °C seems to be highly viscous enough to hold its shape, even though it is not a solid glass but a supercooled liquid at this temperature. The viscosity of the glass at 280 °C was extrapolated to be $10^{7.5}$ Pa s from the logarithmic plot of viscosity against T_g/T, based on the viscosities at T_g and T_d (see ESI). This value was an order of magnitude higher than the viscosity at softening temperature ($10^{6.6}$ Pa s).[38] This indicates that 36H-glass does not deform at 280 °C under its own weight, and it is practically applicable as a “solid” electrolyte in fuel cells, when it is sufficiently stable under fuel cell operation condition. On the other hand, the viscosity

of the glass at 400 °C was also estimated to be ~10^4 Pa s from the logarithmic plot of viscosity against T_g/T. Because this value is 2~3 orders of magnitude smaller than the viscosity at softening temperature, the glass may not be able to maintain its shape at 400 °C. In fact, the shape of the glass sample changed at the temperatures higher than 360 °C (Figs. S2 (f) and (h)), but it did not change at $T \leq 320$ °C as shown in Figs. S2 (b) and (d). Therefore, the conductivities shown in Fig. 3 in the temperature range between 150 and 320 °C are quite reliable.

Fig. 5(a) and (b) show the Raman spectra of the 36H-glass samples before and after measurement of the time evolution of their electrical conductivity at different temperatures. The assignments of the observed bands are summarized in Table 1.[39-45] The Raman spectra of the glasses after being held at 280, 320, 360, and 400 °C were almost identical to that of the glass before conductivity measurement, indicating that no marked structural change occurred during their holding at high temperatures. This means that 36H-glass is thermally stable, as expected; however, closer observation revealed that small sharp peaks appeared at 400–600 cm^{-1} in the spectrum of the glass held at 400 °C for 152 h (inset of Fig. 5(a)) and the band at ~700 cm^{-1} shifted to lower frequency in the spectra of the glasses held at ≥320 °C (Fig. 5(b)). The small peaks that appeared in the Raman spectrum of the glass held at 400 °C are attributed to the formation of a crystalline phase because of their sharpness; therefore, a very small amount of the glass phase crystallized when the sample was held at 400 °C. Unfortunately, the origin of these peaks could not be identified because of their low intensities. We also demonstrated XRD measurement of the glass held at 400 °C (Fig. S3 in ESI), but no sharp peaks appeared in its XRD pattern and we could not identify the crystalline phase formed after the conductivity measurement at 400 °C. According to a previous study of the electrical

conductivity of a proton-conducting phosphate glass,[20] the increase in conductivity observed when the sample was held at high temperatures above T_g was attributed to the formation of phosphoric acid accompanied with phase separation or crystallization, and the decrease in conductivity was attributed to deprotonation accompanied with crystallization or phase separation or the vaporization of phosphoric acid. Therefore, we concluded that a phase transformation definitely began to occur in the glass held at 400 °C. In order to determine the crystallization temperature, T_c, we demonstrated differential thermal analysis, but no exothermic peak was observed at T<450 °C (Fig. S4 in ESI). The sample foamed at T>450 °C by the strong evolution of water vapor due to deprotonation that is accelerated at high temperature; therefore, T_c could not be determined.

In the Raman spectra of the glasses held at 280, 320, and 360 °C, no peaks attributed to crystalline phases were observed, indicating that the glasses did not crystallize. However, the band at ~700 cm^{-1} shifted to slightly lower frequency in the spectra of the glasses held at 320 and 360 °C (Fig. 5(b) and Table 1). It is known that the band at ~700 cm^{-1} that is attributed to stretching vibrations of the P–O–P linkage of $(PO_3^-)_n$ chains ($\nu_{P-O-P,sym}(Q^2)$) shifts to lower frequency as the length of the $(PO_3^-)_n$ chain increases; i.e., as $(PO_3^-)_n$ chains develop polymerization.[24,46] When the deprotonation of the glass occurs according to the following dehydration reaction (2), polymerization of the $(PO_3^-)_n$ chains develops and length of the $(PO_3^-)_n$ chains increases.

$$\equiv P{-}OH + HO{-}P\equiv \rightarrow \equiv P{-}O{-}P\equiv + H_2O \qquad (2)$$

It is also well known that the symmetric and asymmetric stretching modes of $P–O^-$ bonds in $(PO_3^-)_n$ chains ($\nu_{PO2,sym}(Q^2)$ and $\nu_{PO2,asym}(Q^2)$, respectively), which appear at around 1160 and 1245 cm^{-1}, respectively, shift to higher frequency as the length of the $(PO_3^-)_n$ chains increases; i.e., as the $(PO_3^-)_n$ chains develop polymerization.[45,47] As seen in Table

1, these two bands shifted to higher frequency after the glass samples were held at ≥320 °C, consistent with the shift of the $\nu_{P-O-P,sym}(Q^2)$ band to lower frequency. Consequently, the shift of the Raman band at ~700 cm^{-1} was attributed to the polymerization of $(PO_3^-)_n$ chains accompanied with dehydration of the glass sample held at temperatures ≥320 °C.

In IR spectra of the glass samples in the ν_{OH} region, as shown in Fig. 6, the absorption coefficients of the ν_{OH} band of the glasses after being held at 320 and 360 °C were obviously smaller than that of the starting glass (Fig. 6(a)). The OH concentrations of the glasses held at 320 and 360 °C (Fig. 6(b)) were of course lower than that of the starting glass. These changes support the dehydration, i.e., deprotonation, of the glass samples held at temperatures ≥320 °C. Thus, we conclude that slow deprotonation occurred in 36H-glass at temperatures ≥320 °C and the decrease in the conductivity of the glass samples held at temperatures ≥320 °C over time observed in Fig. 4 originated from the decreasing proton carrier concentration.

In contrast, the Raman spectrum of the glass sample after the conductivity measurement at 280 °C for 555 h was identical to that of the starting glass (see Fig. 5(a) and (b) and Table 1), and the IR spectrum of this sample indicated that its OH concentration did not change after holding at 280 °C for 555 h (Fig. 6(b)). These observations reveal that 36H-glass is highly stable at 280 °C for a long period, resulting in the stable proton conductivity of 1×10^{-3} S cm^{-1} at 280 °C observed in Fig. 4. The proton conductivity of 1×10^{-3} S cm^{-1} at 280 °C is the highest reported to date for a proton-conducting phosphate glass,[11-24] although the conductivity is still an order of magnitude smaller than that required for the electrolytes of fuel cells. This indicates that the working hypothesis described in Section 2 is valid to explore proton-conducting phosphate glasses that realize

both high proton mobility and high thermal stability at intermediate temperatures.

Fig. 7 shows the electrical conductivity of 36H-glass as a function of p_{O2}. The conductivity remained constant at 1×10^{-3} S cm^{-1} over a wide p_{O2} range between 1.0×10^{-45} and 1 atm. Considering that the mean transport number of protons under hydrogen atmosphere was determined to be unity from emf measurements, this observation clearly indicates that no electronic conduction occurred in 36H-glass under both strongly reducing and oxidizing conditions. For the conventional proton conductors BZY and BCY, their electron–hole conduction under oxidizing atmosphere induces serious current leakage when these materials are used as electrolytes in fuel cells.[7-10] Therefore, proton conductivity with a mean transport number of unity that is not dependent on p_{O2} is a strong advantage for the application of proton-conducting phosphate glasses, such as 36H-glass, as electrolytes in fuel cells, because a very thin electrolyte layer can be used without current leakage.

4.3. Stability of 36H-glass under fuel cell operating conditions

Fig. 8 displays the current (*I*)–voltage (*V*) curve and corresponding power density of a single fuel cell operated at 280 °C with 36H-glass as the electrolyte. Before continuous operation for 187 h, the open circuit voltage (OCV) was 0.97 V, which is slightly lower than the theoretical voltage of 1.23 V under the present conditions. Because the glass electrolyte had no cracks and did not exhibit electronic conduction, the slightly lower OCV than the theoretical value must originate from failure of the gas-tight seal. Before continuous fuel cell operation, as the output current increased, the cell voltage initially decreased steeply and then displayed an almost linear relation. The *I*-*V* curve revealed that the cell generated a maximum power density of 1.44 mW cm^{-2}. The resistivity of the

electrolyte, i.e., ohmic loss of the fuel cell, was calculated to be 36 Ωcm^2 from its conductivity of 1×10^{-3} S cm^{-1} and thickness of 0.36 mm. These values result in a maximum power density of 6.5 mW cm^{-2} assuming no electrode polarization resistance, which is much larger than the observed maximum power density. This discrepancy is caused by the large activation loss, i.e., the electrode polarization resistance, as shown in Fig. 8 and 9. During the continuous fuel cell operation at 280 °C for 187 h at an output cell voltage of 0.7 V, the output current density decreased gradually over time (Fig. S5 in ESI). After continuous fuel cell operation, the maximum power density decreased to 0.12 mW cm^{-2}, which is approximately 10% of that before continuous fuel cell operation. The decrease of the output power of the fuel cell during continuous operation was suspected to result from the degradation of the glass electrolyte under the fuel cell operation conditions because of the large gradients of oxygen and hydrogen potential in the electrolyte and exposure to water vapor at the cathode. However, the impedance plots of the cell before and after continuous operation shown in Fig. 9 indicate that the ohmic resistance of the glass electrolyte after the continuous fuel cell operation was 220 Ω, which was approximately the same as that before continuous operation. This result indicates that the glass electrolyte remained stable under the fuel cell operating conditions. Raman spectra of the glass electrolyte measured before and after continuous operation were identical, as shown in Fig. 10. This also suggests that no degradation occurs in the glass electrolyte under the fuel cell operating conditions. The decrease of the output power of the cell was able to be attributed to the degradation of the electrode from the observation that the electrode polarization resistance after the continuous operation, corresponding to the arc in the low frequency region, was much larger than that before continuous operation (inset of Fig. 9). These observations indicate that 36H-glass exhibits

good stability under the fuel cell operating conditions. Therefore, we successfully developed a proton-conducting phosphate glass that exhibits fairly high proton conductivity and good stability. Of course, further improvements to increase proton conductivity and to develop suitable electrode materials exhibiting small polarization resistance are required to realize practically applicable ITFCs. The working hypothesis proposed in the present study will help us to develop glass electrolytes suitable for ITFCs.

5. Conclusions

In this study, we proposed a working hypothesis to design precursor phosphate glasses used to obtain proton-conducting phosphate glasses exhibiting both high proton conductivity and high stability at intermediate temperatures after APS as follows:

(i) The concentration of $NaO_{1/2}$ in the precursor glass must be higher than 35 mol%.

(ii) The O/P ratio of the glass composition cannot exceed 3.5.

(iii) The glass network modifier oxides need to contain cations with low electronegativity.

(iv) The glass must contain a sufficient amount of glass network modifiers and intermediate oxides, such as alkaline-earth oxides, Al_2O_3, Y_2O_3, La_2O_3, WO_3, Nb_2O_5, and Ta_2O_5.

(v) The glass should consist of more than four or five components.

(vi) The glass needs to contain a small amount of GeO_2 and/or B_2O_3.

Based on this working hypothesis, we obtained 36H-glass by APS. The proton conductivity of 36H-glass was 1×10^{-3} S cm^{-1} at 280 °C and remained stable for a long time under fuel cell operating conditions. The proton conductivity of 36H-glass is the highest reported for a proton-conducting phosphate glass that works around 300 °C,

indicating that the working hypothesis developed here is useful to develop new proton-conducting glass electrolytes that work at intermediate temperatures.

The proton conductivity of 36H-glass is still an order of magnitude smaller than that required for practical electrolytes of ITFCs; however, the glass exhibits pure proton conduction even in air, resulting in no leakage current, unlike the case for BZY and BCY. This feature should enable fabrication of fuel cells consisting of electrode-supported electrolytes with a very thin thickness, such as one micrometer or less, because the glass thickness can easily be decreased using various techniques; this will achieve very low electrolyte resistance. Consequently, proton-conducting phosphate glasses may be an important material to realize ITFCs, although some of their properties still need to be improved.

Conflicts of interest

There are no conflicts to declare.

Acknowledgment

This work was supported in part by the Advanced Low Carbon Technology Research and Developing Program of the Japan Science and Technology Agency (JST-ALCA), a Grant-in-Aid for Scientific Research of Challenging Exploratory Research (Grant No. 15K14126), and a Grant-in-Aid for the Japan Society for the Promotion of Science (JSPS) Fellows (Grant No. 17J07530). This work was partly performed under the Cooperative Research Program of the "Network Joint Research Center for Materials and Devices" (Nos. 20163006, 20173019, and 20183028) and "Dynamic Alliance for Open Innovation Bridging Human, Environment, and Materials".

References

1. D. J. L. Brett, A. Atkinson, N. P. Brandon and S. J. Skinner, *Chem. Soc. R*ev., 2008, **37**, 1568.
2. B. Zhu, *J. Power Sources*, 2001, **93**, 82.
3. J. P. P. Huijsmans, F. P. F. Berkel and G. M. Christie, *J. Power Sources*, 1998, **71**, 107.
4. K-S. Lee, *J. Phys. Chem. Solids*, 1996, **57**, 333.
5. J. Otomo, N. Minagawa, C-j. Wen, K. Eguchi and H. Takahashi, *Solid State Ionics*, 2003, **156**, 357.
6. D. A. Boysen, T. Uda, C. R. I. Chisholm and S. M. Haile, *Science*, 2004, **303**, 68.
7. K. Nomura and H. Kageyama, *Solid State Ionics*, 2007, **178**, 661.
8. D. Han, Y. Noda, T. Onishi, N. hatada, M. Majima and T. Uda, *Int. J. Hydrogen Energy*, 2016, **41**, 14897.
9. A. Tomita, K. Tsunekawa, T. Hibino, S. Teranishi, Y. Tachi and M. Sano, *Solid State Ionics*, 2006, **177**, 2951.
10. M. Oishi, S. Akoshima, K. Yashiro, K. Sato, J. Mizusaki and T. Kawada, *Solid State Ionics*, 2008, **179**, 2240.
11. H. Namikawa and Y. Asahara, *J. Ceram. Assoc. Jpn.*, 1966, **74**, 27.
12. Y. Abe, H. Shimakawa and L. L. Hench, *J. Non-Cryst. Solids*, 1982, **51**, 357.
13. Y. Abe, H. Hosono, Y. Ohta and L. L. Hench, *Phys. Rev. B: Condens. Matter Mater. Phys.*, 1988, **38**, 10166.
14. H. Takahashi, A. Shimizu and T. Sakuma, *J. Phys. Soc. Jpn.*, 2010, **79**, 115.
15. G. Harley and L. C. Jonghe, *Solid State Ionics*, 2010, **181**, 424.
16. H. Sumi, Y. Nakano, Y. Fujishiro and T. Kasuga, *Solid State Sci.*, 2015, **45**, 5.

17. T. Ishiyama, S. Suzuki, J. Nishii, T. Yamashita, H. Kawazoe and T. Omata, *J. Electrochem. Soc.*, 2013, **160**, E143.
18. T. Ishiyama, S. Suzuki, J. Nishii, T. Yamashita, H. Kawazoe, and T. Omata, *Solid State Ionics*, 2014, **262**, 856.
19. T. Ishiyama, J. Nishii, T. Yamashita, H. Kawazoe and T. Omata, *J. Mater. Chem. A*, 2014, **2**, 3940.
20. K. Kawaguchi, T. Yamaguchi, T. Omata, T. Yamashita, H. Kawazoe and J. Nishii, *Phys. Chem. Chem. Phys.*, 2015, **17**, 22855.
21. T. Yamaguchi, T. Ishiyama, K. Sakuragi, J. Nishii, T. Yamashita, H. Kawazoe and T. Omata, *Solid State Ionics*, 2015, **275**, 62.
22. T. Yamaguchi, T. Ishiyama, K. Sakuragi, J. Nishii, T. Yamashita, H. Kawazoe, N. Kuwata, J. Kawamura and T Omata, *Solid State Ionics*, 2016, **288**, 281.
23. T. Yamaguchi, Y. Saito, Y. Kuwahara, H. Yamashita, T. Ishiyama, J. Nishii, T. Yamashita, H. Kawazoe and T. Omata, *J. Mater. Chem. A*, 2017, **5**, 12385.
24. T. Yamaguchi, T. Kataoka, S. Tsukuda, T. Ishiyama, J. Nishii, T. Yamashita, H. Kawazoe and T. Omata, *Phys. Chem. Chem. Phys.*, 2017, **19**, 29669.
25. W. Vogel, *Glass Chemistry*, Springer-Verlag, Berlin, 2nd edn, 1994, pp. 120-122.
26. Y.-M. Sung, *J. Mater. Res.*, 2002, **17**, 517.
27. G. Harley, K. D. Kreuer, J. Maier and L. C. Jonghe, *J. Non-Cryst. Solids.*, 2009, **355**, 932.
28. R. K. Brow and D. R. Tallant, *J. Non-Cryst. Solids.*, 1997, **222**, 396.
29. R. Millini, G. Perego and G. Bellussi, *Top. Catal.*, 1999, **9**, 13.
30. S. -J. Hwang, C. -Y. Chen and S. I. Zones, *J. Phys. Chem. B*, 2004, **108**, 18535.

31. J. A. van Bokhoven, A. M. J. van der Eerden and D. C. Koningsberger, *J. Am. Chem. Soc.*, 2003, **125**, 7435.
32. Y. Aoki, H. Habazaki and T. Kunitake, *J. Am. Chem. Soc.*, 2009, **131**, 14399.
33. Y. Abe and D. E. Clark, *J. Mater. Sci. Lett.*, 1990, **9**, 244.
34. J. E. Shelby, *J. Non-Cryst. Solids.*, 1982, **49**, 287.
35. Y. Hattori, T. Wakasugi, H. Shiomi, J. Nishii and K. Kadono, *J. Mater. Res.*, 2012, **27**, 999.
36. H. Hayashi, E. Shudo, J. Kawamura and Y. Nakamura, *J. Non-Cryst. Solids*, 1998, **242**, 33.
37. J. Kawamura and M. Shimoji, *J. Non-Cryst. Solids*, 1986, **88**, 281.
38. J. E. Shelby, Introduction to Glass Science and Technology, 2nd edn, 2005, p. 112.
39. M. G. Donato, M. Gagliardi, L. Sirleto, G. Messina, A. A. Lipovskii, D. K. Tagantsev and G. C. Righini, *Appl. Phys. Lett.*, 2010, **97**, 231111.
40. K. Fukumi and S. Sakka, *J. Mater. Sci.*, 1988, **23**, 2819.
41. A. El. Jazouli, J. C. Viala, C. Parent, G. Le Flem and P. Hagenmuller, *J. Solid State Chem.*, 1988, **73**, 433.
42. J. M. Jehng and I. E. Wachs, *Chem. Mater.*, 1991, **3**, 100.
43. R. K. Brow, *J. Non-Cryst. Solids*, 2000, **263–264**, 1.
44. R. K. Brow, D. R. Tallant, J. J. Hudgens, S. W. Martin and A. D. Irwin, *J. Non-Cryst. Solids*, 1994, **177**, 221.
45. M. Tatsumisago, Y. Kowada and T. Minami, *Phys. Chem. Glasses*, 1988, **29**, 63.
46. J. E. Pemberton and L. Latifzadeh, *Chem. Mater.*, 1991, **3**, 195.
47. M. A. Karakassides, A. Saranti, I. Koutselas, *J. Non-Cryst. Solids*, 2004, **347**, 69.

Tables

Table 1 Assignments of the bands observed in Raman spectra of the glass samples before and after conductivity measurements at 280, 320, 360, and 400 °C.

Position / cm^{-1}						
Starting	280 °C for 555h	320 °C for 454h	360 °C for 332h	400 °C for 152h	Assignments	Ref.
291	291	290	290	291	Bending mode of O−Nb−O bond of NbO_6 octahedra, δ_{O-Nb-O}	39-42
508	508	508	507	–	Combination mode of the O−Nb−O bending mode with the O−P−O bending mode, $\delta_{O-Nb-O} + \delta_{O-P-O}$	39-42
604	604	604	605	604	Stretching mode of Nb−O bond of NbO_6 tetrahedra, ν_{NbO}	39-42
718	717	715	713	702	Symmetric stretching mode of P−O−P linkage for $(PO_3^-)_n$ chain, $\nu_{P-O-P,sym}(Q^2)$	43-45
924	924	926	930	935	Stretching mode of Nb−O^- bond of NbO_6 tetrahedra, ν_{NbO^-}	39-42
1031	1032	1031	1032	1035	Symmetric stretching mode of P−O^- bond for $P_2O_7^{4-}$ ion, $\nu_{PO3,sym}(Q^1)$	43-45
1161	1162	1164	1176	1174 1153	Symmetric stretching mode of P−O^- bond for $(PO_3^-)_n$ chain, $\nu_{PO2,sym}(Q^2)$	43-45
1244	1245	1246	1253	1258	Asymmetric stretching mode of P−O^- bond for $(PO_3^-)_n$ chain, $\nu_{PO2,asym}(Q^2)$	43-45
1312	1310	1312	1319	1322	Stretching mode of P=O bond, $\nu_{P=O}(Q^3)$	43-45

Figures

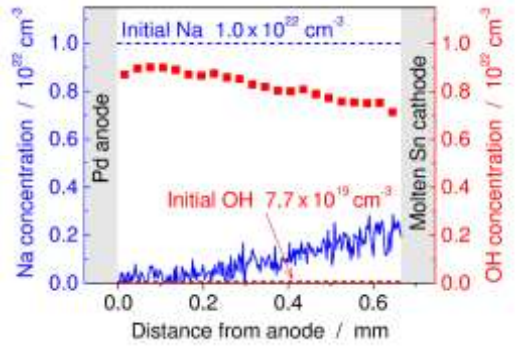

Fig. 1 Concentration depth profiles of Na (blue line) and OH (red squares) in 36Na-glass after APS determined from EDX and IR spectroscopy. The blue and red dashed lines indicate Na and OH concentrations in 36Na-glass before APS, respectively.

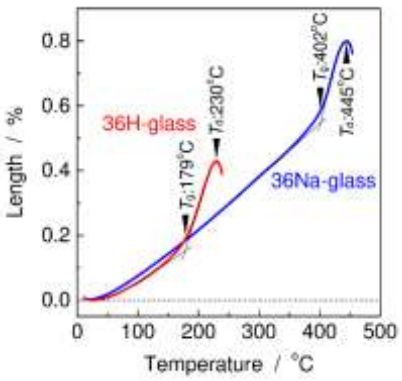

Fig. 2 Thermal expansion curves of 36H-glass (red line) and 36Na-glass (blue line) measured in air.

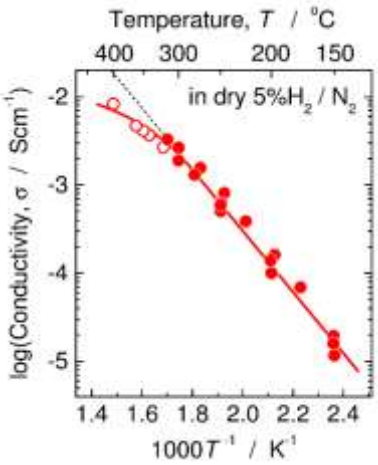

Fig. 3 Arrhenius plot of the proton conductivity of 36H-glass measured under dry 5% H_2/95% N_2 atmosphere. The black dashed line was extrapolated from the data in the temperature range of 150–300 °C. The conductivities at T>320 °C involves the contribution of the inaccuracy of the dimension of the glass sample as seen in Fig. S2 in ESI; therefore, the data is distinguished by open dots.

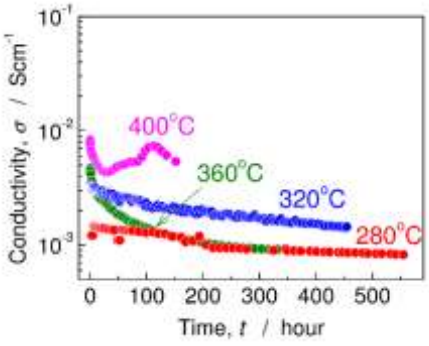

Fig. 4 Time evolution of the proton conductivity of 36H-glass samples held at 280, 320, 360, and 400 °C. The conductivities at 360 and 400°C involves the contribution of the inaccuracy of the dimension of the glass sample as seen in Fig. S2 in ESI.

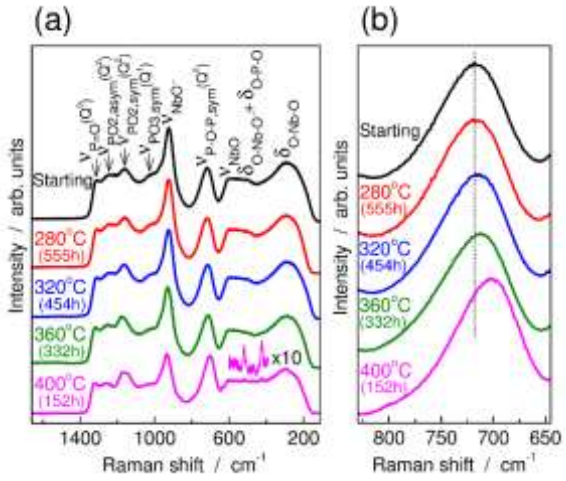

Fig. 5 (a) Raman spectra of the glass samples before and after the conductivity measurements at 280, 320, 360, and 400 °C. (b) Enlarged view of the Raman spectra in the region of the symmetric stretching mode of the P–O–P linkage of the $(PO_3^-)_n$ chain ($\nu_{P-O-P,sym}(Q^2)$).

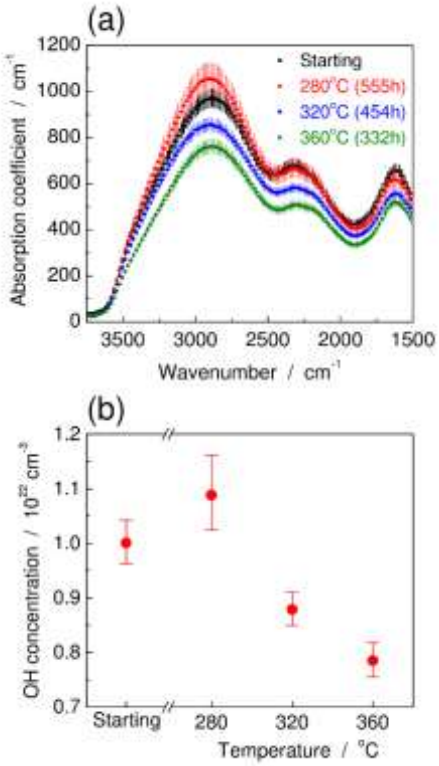

Fig. 6 (a) IR spectra in the region of the O–H stretching vibration (ν_{OH}) of the glass samples before and after the conductivity measurements at 280, 320, and 360 °C. (b) The OH concentration of the glass samples determined from the ν_{OH} absorption in IR spectra.

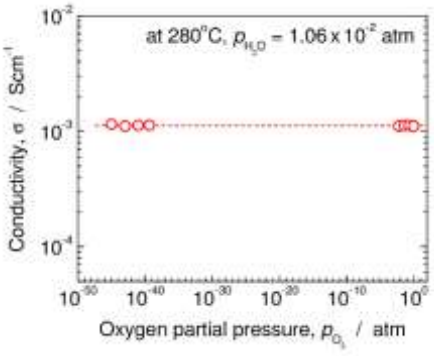

Fig. 7 Electrical conductivity of 36H-glass at 280 °C as a function of p_{O2}.

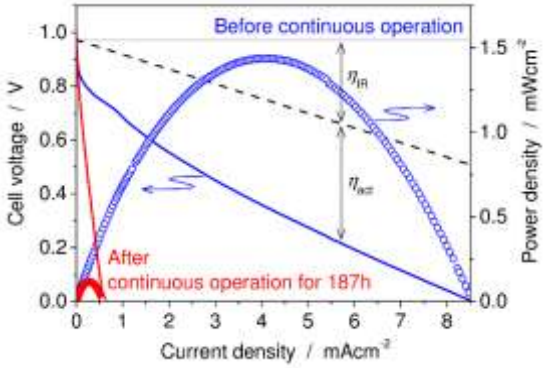

Fig. 8 I-V curve of an ITFC with a structure of dry 100% H_2, Pd | 36H-glass | Pd, dry air before (blue line and open circles) and after (red line and closed circles) operation for 187 h at 280 °C. η_{IR} and η_{act} in the figure indicates the ohmic loss coming from the electrolyte resistance and the activation loss coming from the polarization resistance of the Pd anode and cathode, respectively. Black broken line in the figure represents the η_{act}-free cell voltage before the continuous operation.

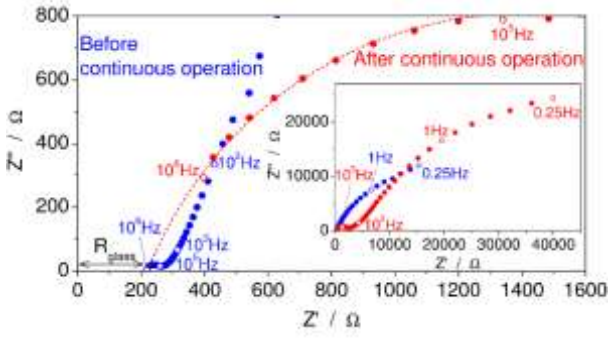

Fig. 9 Impedance plots of the ITFC before (blue dots) and after (red dots) operation for 187 h. The red dashed line is the fitting line of the red dots.

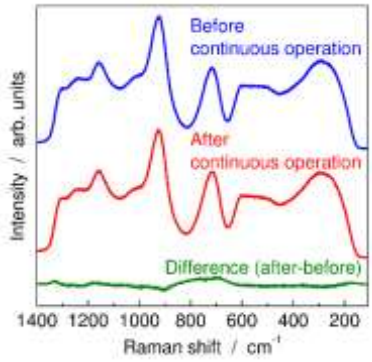

Fig. 10 Raman spectra of 36H-glass before (blue line) and after (red line) ITFC operation for 187 h. The green line is the difference spectrum.

Table of contents (maximum 20 words)

$36HO_{1/2}$-$4NbO_{5/2}$-$2BaO$-$4LaO_{3/2}$-$4GeO_2$-$1BO_{3/2}$-$49PO_{5/2}$ glass exhibits proton conductivity of 1×10^{-3} S cm^{-1} at 280 °C and is stable under fuel cell operating conditions.